Cold Regions Science and Technology 218 (2024) 104056

Contents lists available at ScienceDirect

Cold Regions Science and Technology

journal homepage: www.elsevier.com/locate/coldregions

Quantifying short-term changes in snow strength due to increasing liquid water content above hydraulic barriers

Mikael Schlumpf [a,*], Jordy Hendrikx [d,e,f], John Stormont [a], Ryan Webb [b,c]

[a] Department of Civil, Construction, and Environmental Engineering, University of New Mexico, Albuquerque, NM 87131, United States
[b] Center for Water and the Environment, University of New Mexico, Albuquerque, NM 87131, United States
[c] Department of Civil and Architectural Engineering and Construction Management, University of Wyoming, Laramie, Wyoming 82071, United States
[d] Antarctica New Zealand, Christchurch 8053, New Zealand
[e] Department of Geosciences, Faculty of Science and Technology, UiT the Arctic University of Norway, P.O. Box 6050, Langnes, 9037 Tromso, Norway
[f] Snow and Avalanche Laboratory, Montana State University, Bozeman, MT, United States

ARTICLE INFO

Keywords:
Wet snow
Slab avalanches
Blade hardness
Shear strength
Liquid water content

ABSTRACT

The rapid weakening of snow layers that accumulate infiltrating liquid water is a well-known, but poorly quantified, mechanism for wet-snow slab avalanche formation. Therefore, quantifying this mechanical process is a crucial part of forecasting these snow avalanches accurately. Currently, studies do not agree on how snow strength should change as a function of volumetric liquid water content (θ) and whether this relationship differs between snow types. Furthermore, strength measurements taken at or above $\theta = 7\%$ in snow are rare, so there is limited understanding at this end of the θ continuum. These levels of saturation can occur in the snow immediately above hydraulic barriers and are considered important for wet-snow slab avalanches to initiate. To address this knowledge gap, a blade hardness gauge (BHG, a.k.a. thin blade penetrometer) and SLF snow sensor were used to take 349 targeted paired measurements of strength and θ, respectively, in the snow above 19 manually wetted hydraulic (capillary) barriers. Using a multiple regression analysis, we developed an expression for the blade hardness of manually wetted snow as a function of θ, crystal form, and blade hardness prior to wetting ($R^2 = 0.85$). To understand these results in terms of a common measure of snow strength, we also performed a comparison of the BHG and a shear frame in dry snow. The two instruments are highly linearly correlated ($R^2 = 0.94$), allowing us to interpret our regression in terms of shear strength when compressive stress is low. Our results demonstrate that short-term (< 2 h) changes in snow strength due to increasing θ can differ between snow layers. These differences can be empirically modelled using easily measured dry snow properties (i.e. crystal form and blade hardness), which could allow avalanche forecasters to be more selective when identifying failure layers in advance of a wetting event.

1. Introduction

Snow avalanches (hereafter also called avalanches) are a significant hazard in mountainous environments around the world. Climate warming is expected to increase the proportion of slab avalanches occurring in wet snow (Castebrunet et al., 2014; Hendrikx et al., 2022; Lazar and Williams, 2008; Pielmeier et al., 2013; Sinickas et al., 2016), yet this destructive type of avalanche remains particularly difficult to predict (Mitterer and Schweizer, 2014). Wet slab avalanches form in response to liquid water in the snowpack, which is introduced by snow melt or rain-on-snow. They initiate during very specific conditions that last for a short period of time (Baggi and Schweizer, 2009), since formation mechanisms are interactive, highly transient, and spatially heterogenous (Conway and Raymond, 1993). To address this complex forecasting challenge, physics-based modeling (e.g. Wever et al., 2016, 2018) has proven more promising than traditional statistical methods, which rely on sparse point observations of meteorological and snowpack data (Baggi and Schweizer, 2009; Mitterer and Schweizer, 2013; Peitzsch et al., 2012). However, the success of these physical models is still limited, primarily because the mechanical processes leading to wet slab avalanche release are poorly quantified.

The formation of any slab avalanche involves the failure of a weak snow layer that sits below a cohesive snow slab (Schweizer et al., 2003). Failure initiates locally, and then rapidly propagates when the fracture

* Corresponding author.
E-mail address: mschlumpf@unm.edu (M. Schlumpf).

https://doi.org/10.1016/j.coldregions.2023.104056
Received 24 May 2023; Received in revised form 17 October 2023; Accepted 28 October 2023
Available online 31 October 2023

exceeds the critical crack length (Gaume et al., 2017). When the snowpack is dry, this process often occurs in response to increasing weak layer stress from external loads (e.g., new snow, humans, explosives) (Schweizer et al., 2003). In contrast, wet slab avalanches are primarily driven by internal changes to the snowpack's mechanical properties, which occur rapidly after liquid water is introduced for the first time (Conway and Raymond, 1993). Specifically, the weakening of snow layers that accumulate infiltrating liquid water is often considered a prerequisite for wet slab avalanche release (Baggi and Schweizer, 2009; Kattelmann, 1985; Marienthal et al., 2012; Reardon, 2008; Wever et al., 2018). Therefore, to improve prediction of these avalanches, a sound understanding of how liquid water affects the strength of snow is necessary.

The strength of dry weak snow layers can be characterized using a modified Mohr-Coulomb (MC) model (Gaume et al., 2017; Reiweger et al., 2015). Above a certain compressive stress, this model deviates from traditional MC behavior to account for failure in both shear and compression. A mixed-mode approach is necessary because weak layer failure can be driven by volumetric collapse (Heierli et al., 2008; van Herwijnen et al., 2010), especially when initiated from low angle or flat terrain (Birkeland et al., 2006). When a dry snow layer becomes wet, the parameters in this model (e.g., cohesion, internal angle of friction, compressive strength) will rapidly change. Liquid water facilitates heat flow between ice surfaces at different equilibrium temperatures, preferentially melting crystals, and inter-crystal ice bonds, with small radii (Colbeck, 1973; Raymond and Tusima, 1979). Since this weakening process is limited by the extent that ice surfaces are connected by liquid water, it is thought to be slow until pore saturation reaches the funicular regime (Colbeck, 1973). This transition occurs near 3–7 % volumetric liquid water content (θ), depending on the snow type (Denoth, 1980). Adding further complexity, bond melting competes with capillary forces, which act to strengthen the snow matrix. The difference in pore air and water pressure can be large in unsaturated snow (Yamaguchi et al., 2010, 2012), leading to a net pressure that pulls wet crystals together. In other unsaturated porous materials like sand, this can dramatically increase shear strength – a phenomenon referred to as capillary cohesion (Lu and Likos, 2004).

Since physically modeling the processes discussed above is complex, previous work has focused on developing empirical relationships between snow strength and θ instead. Typically, a shear frame (Perla et al., 1982) has been used to measure the shear strength of wet snow under low compressive stress (e.g. Bhutiyani, 1996; Brun and Rey, 1987; Yamanoi and Endo, 2002). However, results from these studies are ambiguous, showing some snow layers that don't change in strength at or below $\theta = 6\%$, and others that decrease in strength continuously. More recently, investigations using a Snow Micro Penetrometer (SMP, Johnson and Schneebeli, 1998) revealed that snow composed of faceted crystals may begin weakening at lower θ and at larger rates than other snow types (Techel et al., 2011). However, this dependence on crystal form is poorly understood and has not been reflected in previous wet snow strength equations (e.g. Yamanoi and Endo, 2002). Another concern is the lack of snow strength measurements taken at or above $\theta = 7\%$. These levels of saturation occur in the snow immediately above hydraulic barriers (e.g. capillary barriers and ice lenses) (Avanzi et al., 2016; Webb et al., 2018) and are considered important for wet slab avalanches to initiate (Baggi and Schweizer, 2009; Kattelmann, 1985; Peitzsch et al., 2012; Wever et al., 2016, 2018). However, measuring these thin areas of saturated snow accurately is difficult, since many traditional strength and liquid water content instruments (e.g. shear frame, snow fork) integrate over too large an area.

Therefore, the goal of this study is to improve empirical models of wet snow strength by using instruments and methods that can target the snow immediately above hydraulic barriers, as liquid water accumulates for the first time. The research objectives are: 1) Determine the relationship between shear frame and blade hardness gauge (BHG, a.k.a. thin blade penetrometer) measurements; 2) Use a BHG and SLF snow sensor to make targeted paired measurements of strength and θ, respectively, in the snow above manually wetted hydraulic barriers; 3) Use statistical methods to express blade hardness, and therefore shear strength, as a function of θ and snow properties prior to wetting (e.g. crystal form).

2. Methods

2.1. Instrumentation

Targeted θ and strength measurements above hydraulic barriers were made using a SLF snow sensor and blade hardness gauge (BHG), respectively. The SLF snow sensor measures snow dielectric permittivity and calculates the density of dry snow, or θ of wet snow, using empirically derived functions (FPGA Company, 2018) that compare well to a recent in situ study (Webb et al., 2021). A capacitive plate, which is sensitive to the presence of ice and water, is placed on top of the snow and a handheld datalogger is used to control and log the measurement (Fig. 1 A). The process is not destructive, so repeated measurements over time of the same snow volume in situ are possible – unlike other liquid water content devices (e.g., snow fork or Denoth meter; Techel and Pielmeier, 2011). Additionally, the SLF snow sensor has a small measurement volume (45 × 95 × 17 mm) (FPGA Company, 2018), minimizing the influence of neighboring snow when measuring θ at thin wet layers, as seen above hydraulic barriers (Eiriksson et al., 2013).

The BHG uses a 100 mm wide, 0.6 mm thick stainless-steel blade attached to a digital push-pull force gauge (Borstad and McClung, 2011). New models of the blade hardness gauge (Barsevskis and Paetkau, 2022) are not currently commercially available, so we constructed one following the original template (Borstad and McClung, 2011) (Fig. 1 B). The blade is inserted into the snow at a fast rate (~10 cm/s) over 5 cm, such that the blade edge is parallel to the snow layer being tested. After insertion, the maximum compressive force measured by the gauge is recorded as the blade hardness in Newtons (Borstad and McClung, 2011). The fast insertion ensures that strain rate effects on the failure stress of snow are small (Borstad and McClung, 2011; Fohn and Camponovo, 1997). We used a Chatillon DFS series force gauge that is rated up to 250 kN, has a resolution of 0.1 N, and has a recommended operating temperature between −1 and 49 °C. The ambient temperature during experiments ranged between −2 and 7 °C.

Although BHG measurements are known to correlate well with several important mechanical properties (Borstad and McClung, 2011, 2013), it is unclear how they relate to shear strength. Therefore, we conducted a dry snow comparison between the BHG and a shear frame (Föhn, 1987; Jamieson and Johnston, 2001; Perla et al., 1982). In contrast to many shear frame studies, where a thin plane of weak snow is tested, we measured the shear strength within thicker, relatively homogeneous snow layers. This facilitated a more robust comparison of the instruments, since we could take measurements in a wider variety of snow types.

We used a shear frame with an area of 25,000 mm^2, a depth of 40 mm, three active cross-members with 53 mm between each member, and a width of 162 mm (Fig. 1 C). This is the preferred frame design of many previous studies (Jamieson and Johnston, 2001; Perla et al., 1982; Sommerfeld, 1984). Within our comparison plot (Fig. 2), snow was removed until ~40 mm (depth of the frame) of snow remained above the middle of the layer of interest. The frame was then gently inserted into the snow until the top of the frame was even with the plot surface. Snow in front of the frame was carefully removed, and a thin blade was passed around the outside edge (Jamieson and Johnston, 2001). A force gauge was then used to pull the frame quickly down-slope, via a cord connecting its sides, until shear fracture occurred. The maximum pull force, in Newtons, measured by the gauge was recorded. Tests were rejected if the time to fracture exceeded one second or if half or more of the fracture surface was not planar (Jamieson and Johnston, 2001).

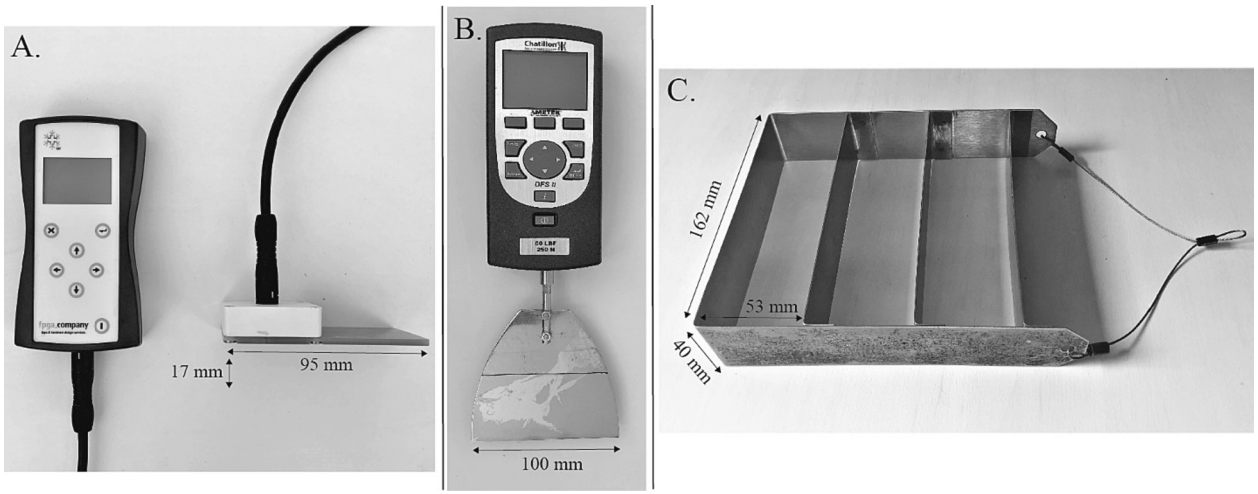

Fig. 1. SLF snow sensor (A), blade hardness gauge (B), and shear frame (C) used in our study. The 17 mm measurement penetration depth for the SLF snow sensor is shown.

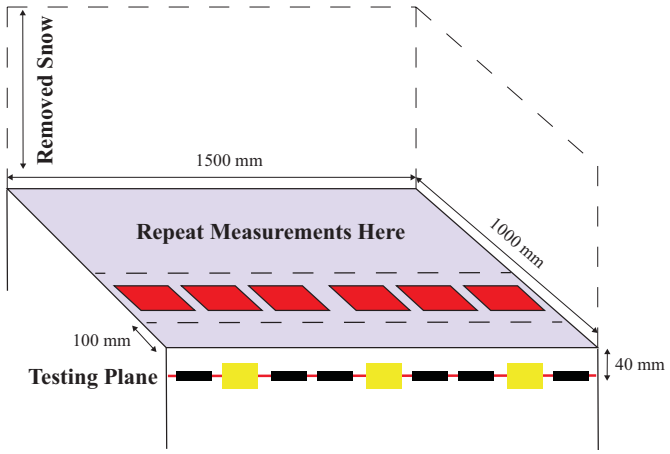

Fig. 2. Plot layout for the shear frame – BHG comparison. Red squares are shear frame measurements, thin black rectangles are BHG measurements, and thicker yellow rectangles are density measurements using a 250 cc cutter. Dotted lines are where the plot area was cut back. (For interpretation of the references to colour in this figure legend, the reader is referred to the web version of this article.)

2.2. Experiment design

2.2.1. BHG – shear frame comparison

The comparison took place on gentle slopes between 15 and 20 degrees. For each snow layer in the comparison, we sampled 12 shear frame measurements (Jamieson and Johnston, 2001), 12 BHG measurements, and 6 density measurements (Fig. 2). Density was measured using a 250 cc Snowmetrics Rip 2 cutter and a Pesola spring scale, and crystal form and size were measured using a 2 mm gridded crystal card and 10× magnifying loupe (Fierz et al., 2009). Six evenly spaced BHG measurements and three density measurements were taken across the front of the prepared plot. BHG measurements were taken ~40 mm below the plot surface to match the testing plane of the shear frame. Next, the plot was cut back 100 mm and 6 shear frame measurements were taken across the front of the new plot. The plot was then cut back again, removing the snow affected by the shear frame, and the whole process was repeated in the remaining plot area.

2.2.2. Wet snow strength

To get repeatable snow strength measurements at a range of liquid water contents, we performed manual wetting experiments using a handheld sprayer filled with a highly diluted, ~0 °C Rhodamine solution. To reduce the effects of incoming short-wave radiation and outgoing long-wave radiation on the temperature at the snow surface, a small shade structure was used above each plot (Fig. 3 A). The shade structure also marked the boundaries of the wetting plot – approximately 800 × 1000 mm – to ensure that the wetted area above each tested layer was the same size.

Once a suitable undisturbed location was selected, we used standard snow pit practices (Fierz et al., 2009) to identify dry hydraulic barriers in the snowpack. Dryness was assessed using a hand wetness test (Fierz and Fohn, 1994). Transitions from fine-grained, high-density snow to coarse-grained, low-density snow were considered possible capillary barriers (Webb et al., 2018) but more subtle textural changes in new snow were also noted (Peitzsch et al., 2008; Schneebeli, 1995). At these types of interfaces, liquid water can accumulate due to the high suction and conductivity of the infiltrated snow above, relative to the snow below (Avanzi et al., 2016). In contrast, permeability barriers (a.k.a hydraulic conductivity barriers) occur when the permeability of a snow layer is less than the rate of infiltrating liquid water (Webb et al., 2018). Ice lenses or melt-freeze crusts were considered possible permeability barriers. Specific hydraulic barriers were chosen for testing based on available time and which snow types (crystal form, size, and density) needed more representation in our data set.

Before wetting, we removed all but ~50 mm of snow from above the chosen hydraulic barrier, within the 800 × 1000 mm plot (Fig. 3 B). On this newly exposed surface, we measured crystal size and shape in at least five different locations to obtain the average dry properties of the snow. Density was also measured in 10 locations using the SLF snow sensor instead of the 250 cc cutter, so that measurements did not damage the wetting surface. Prior to wetting, the snow temperature above the barrier was measured using a digital thermometer. The snow was left to warm until it was between −1 and 0 °C and then dry blade hardness measurements were taken across the front of the plot, just above the barrier. This was done to minimize temperature-induced strength differences between the dry and wet states of the snow (Roch, 1965; Schweizer, 1998).

The manual wetting took place over 3–4 consecutive trials. For each trial, we mixed 0°C water with a few drops of diluted Rhodamine in a 1.5 L garden sprayer. Using the sprayer, we evenly applied 0.5–1.0 L (0.6–1.3 mm equivalent rain) of the dyed solution to the plot surface at a rate of ~0.4 L/min (~29 mm/h equivalent rain rate). We slightly varied the volume of applied water during each trial depending on the liquid water content we were hoping to achieve. We recorded the time that

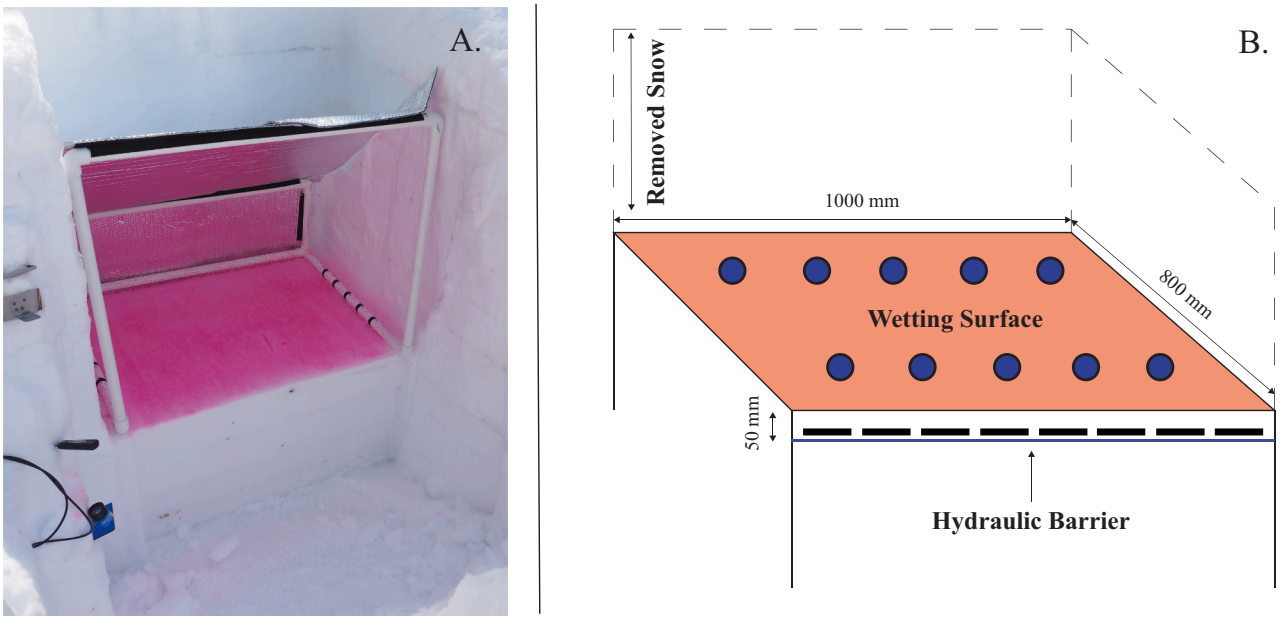

Fig. 3. (A) The shade structure and wetting plot immediately after the first wetting trial. In this photo, accumulation above the barrier hasn't begun. (B) The diagram illustrates how dry measurements were taken prior to wetting. Blue circles represent density measurements using the SLF snow sensor and thin black rectangles are dry blade hardness measurements. Crystal form and size were also measured on the plot surface prior to wetting. (For interpretation of the references to colour in this figure legend, the reader is referred to the web version of this article.)

spraying began, and the water was allowed to infiltrate and spread across the barrier for 10–15 min after the spraying ended. Since water was applied at a fast rate to an initially dry snowpack, flow to the barrier always occurred in discrete and narrow vertical flow paths (Avanzi et al., 2016; Peitzsch et al., 2008; Waldner et al., 2004). This meant that, although water spread across the barrier laterally, much of the snow between the barrier and the wetting surface was usually left dry (Fig. 4 A).

After the infiltration period, the wet snow above the barrier was consistently very thin (around 10 mm, although this was not measured), since liquid water would move laterally after a certain amount of vertical accumulation. This thin layer of dyed wet snow was usually visible on the face of the wetting plot. We gently removed all but ~10 mm of excess dry (un-dyed) snow from above these wet areas using a putty knife, allowing us to see the lateral distribution of wetted snow from above without damaging it (Fig. 4 B). The SLF snow sensor was then placed directly above an evenly dyed area for a targeted permittivity measurement (Fig. 4 B). With ~10 mm of dry snow left above the wet layer, most, if not all the wet snow's thickness was captured by the SLF snow sensor's 17 mm vertical measurement distance. Each permittivity

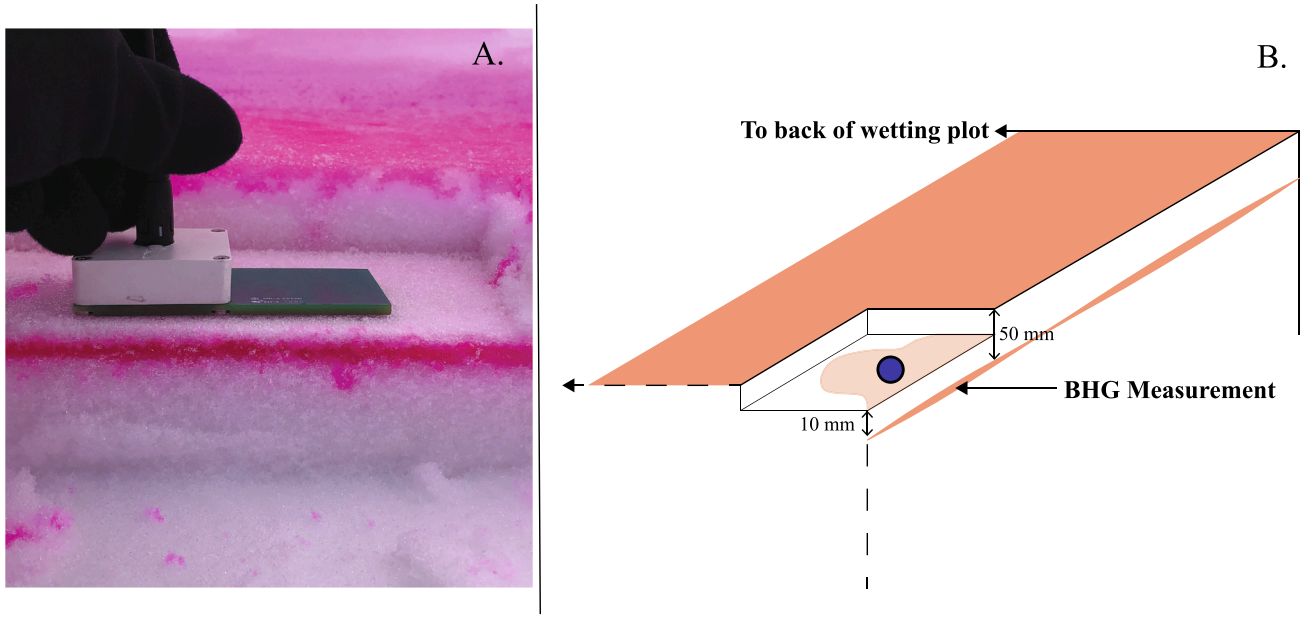

Fig. 4. (A) Targeted permittivity measurement is being taken directly above a wet portion of snow at a capillary barrier after all but ~10 mm of snow was removed. Note that the snow above the wet barrier is dry since water was transported through narrow preferential flow paths. (B) Schematic depicts how paired measurements were made and how wet areas were slightly visible from above due to the dye. The blue circle represents a permittivity measurement using the SLF snow sensor. (For interpretation of the references to colour in this figure legend, the reader is referred to the web version of this article.)

measurement was followed by a paired BHG measurement, where the blade was inserted into the face of the plot in front of the portion of wet snow measured by the SLF snow sensor.

Once several paired measurements were made (typically five), we cut back the portion of the wetting plot that was just measured and began the next wetting trial using the remaining area (Fig. 5). Trials continued until there was insufficient space in the study plot to wet. Each trial added additional water to the wet snow above the barrier, allowing for measurements of increasingly saturated snow. The total time for 3–4 wetting trials above a single barrier was less than 2 h.

2.3. Research location, terrain, and conditions

We collected data at five field sites over eleven days in the mountains of northern New Mexico and southern Colorado, in the southwestern United States (for site and condition details see: Schlumpf et al., 2023). These mountains are characterized by a cold and dry continental climate, with large diurnal changes in temperature due to their southern latitude and high elevation. For most of the snow season, this promotes a snowpack dominated by kinetic metamorphism and the growth of faceted crystals, both at the snowpack base and the surface (Birkeland, 1998). Additionally, mid-winter warm spells are common, causing melt water to infiltrate a dry and highly layered snowpack.

The wetting experiments took place in flat terrain at or below tree line. Specific locations were chosen based on where we expected to find hydraulic barriers and the snow types that lacked representation in our dataset. Plots varied from open, wind-blown meadows, to sheltered areas adjacent to dense forest. Data were collected in March and April of 2021 and 2022, during warm spells when air temperatures were above freezing.

2.4. Data analysis

The R software environment, version 4.2.2, was used for all data analysis.

2.4.1. BHG – shear frame comparison

A total of 18 dry snow layers were measured for the comparison of the two instruments, resulting in 216 shear frame and 216 BHG measurements (Schlumpf et al., 2023). For each layer, the first two shear frame measurements were discarded (Jamieson and Johnston, 2001) to allow adjustment to the pull force required for failure. We also discarded the first two BHG measurements to equalize the number of measurements from each instrument. We calculated shear stress at failure, in kPa, by dividing shear frame force measurements by the frame area, in m^2, and multiplying by 1000. We also added the shear stress contributed by the mass of the overlying snow and frame, although this component was small and had a negligible impact on our analysis. Since shear frame measurements are sensitive to the size of the tested area (Fôhn, 1987; Jamieson and Johnston, 2001; Sommerfeld, 1984), we used an empirical equation (Fôhn, 1987) to adjust our measurements to the strength of an arbitrarily large failure area – known as the Daniels strength (Sommerfeld, 1980). We will refer to the Daniels strength as the shear strength of the snow layer, denoted as τ_f.

Correlations between the mean blade hardness (B_{avg}), mean shear strength ($(\tau_f)_{avg}$), and mean density (ρ_{avg}) of the layers were explored using Spearman's rank correlation coefficients (r_s) and their associated p-values. We also compared the mean values from each instrument using a linear regression model, where $(\tau_f)_{avg}$ was the response variable and B_{avg} was the predictor.

We compared the variability of shear frame measurements to those from the BHG by calculating the coefficient of variation (CV) from both instruments for each of the 18 layers. The CV is the preferred measure of variability for snow strength since it is less dependent on mean strength than other measures (Jamieson and Johnston, 2001). We used a one-sided sign test to compare the median CV values across all layers. We chose a non-parametric test because there was one influential CV outlier in the blade hardness dataset.

2.4.2. Wet snow strength analysis

After developing our methods in 2021, we tested the snow above 20 capillary barriers in March and April of 2022. Permeability barriers did not reliably accumulate liquid water in our experiments, agreeing with previous studies (Eiriksson et al., 2013). We removed one layer from our analysis, whose average dry blade hardness (32 N) was a significant outlier. This left 349 paired permittivity-BHG measurements taken in 19 different snow layers (Schlumpf et al., 2023). Permittivity measurements were converted to θ using the empirical equations developed by the SLF snow sensor manufacturer (FPGA Company, 2018). In these equations, dry density needs to be specified. For a given layer, we used the mean of 10 dry density measurements (ρ_{dry}) taken using the SLF snow sensor. Although calculating density using permittivity is subject to larger errors (Webb et al., 2021), we preferred this method over the 250 cc sampler, since measurements were taken directly on the wetting surface.

We performed a multiple regression analysis to quantify the relationship between wet blade hardness (B) in Newtons, θ, and dry snow layer properties. The properties that we chose (Fig. 6, Table 1) were the

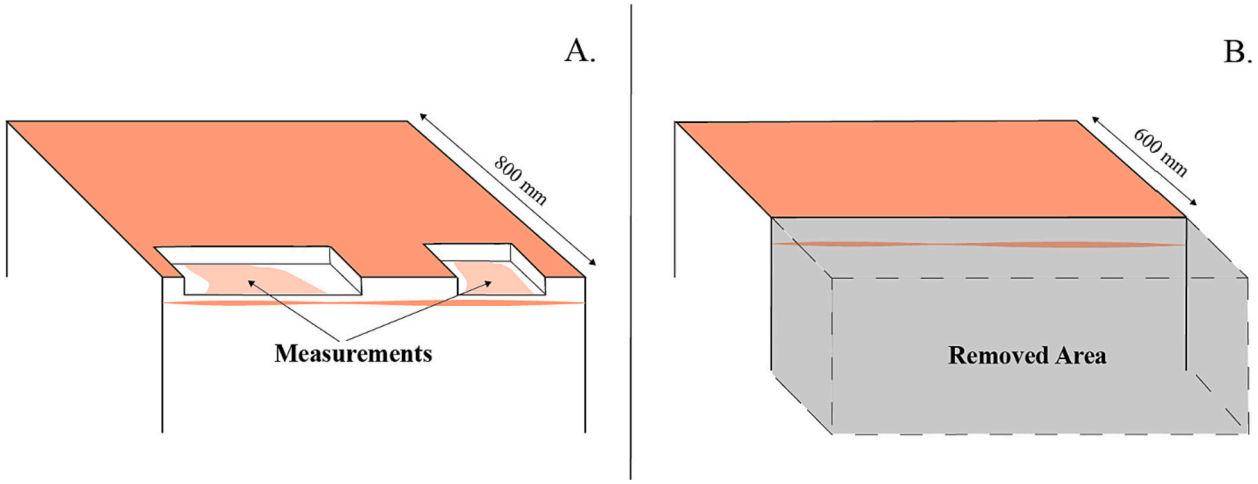

Fig. 5. (A) An example of the wetting plot after measurements were made during the first wetting trial. (B) Cutting back the portion of the wetting plot that was affected by measurements in the first trial, before beginning the second trial.

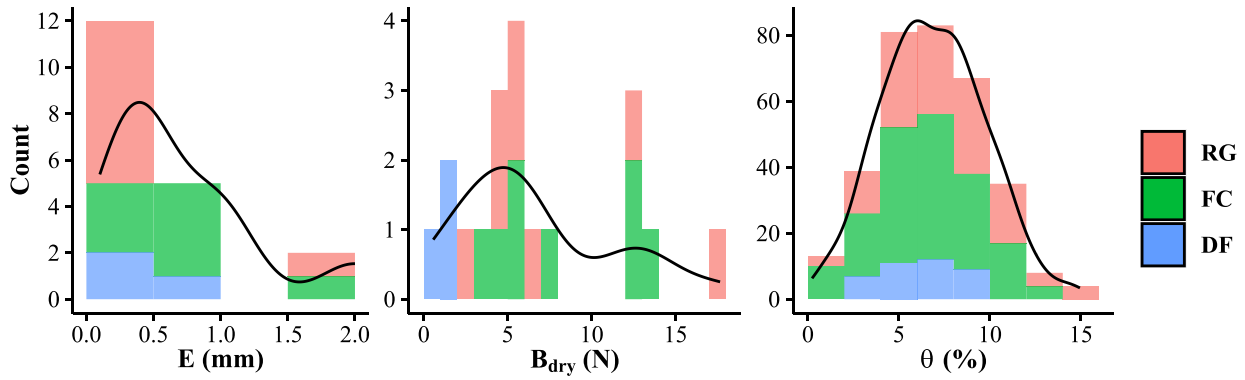

Fig. 6. Distribution of variables used in our regression analysis organized by primary crystal form. RG, FC, and DF represent rounded, faceted, and decomposing fragmented crystal forms, respectively. See Table 1 for an explanation of all variables.

Table 1
Variables involved in our wet snow strength analysis and their units/precision.

Description	*Variable*	*Units*	*Precision*
Average crystal size	E	mm	0.1
Primary crystal form	F	N/A	N/A
Average dry density using SLF snow sensor	ρ_{dry}	kg/m^3	1
Average dry blade hardness	B_{dry}	Newtons	0.1
Blade hardness	B	Newtons	0.1
Volumetric liquid water content	θ	vol. %	0.1

average dry blade hardness (B_{dry}), primary crystal form (F), and average crystal size (E), as we expected these variables to affect capillary cohesion and bond melting rates (Colbeck, 1973; Yamaguchi et al., 2012). ρ_{dry} was not included as a predictor because it was highly correlated ($r_s = 0.91, p < 10^{-16}$) with B_{dry}. Following the approach of other wet snow strength studies (Yamanoi and Endo, 2002), we used the natural logarithm of B as our response variable, which improved its normality. Since we knew that B should equal B_{dry} when θ is 0, we set the regression intercept to $ln(B_{dry})$ and allowed B_{dry}, F, and E to change the regression slope with respect to θ. We expected that the effects of B_{dry} and F on the slope could be interdependent, so we included these terms as an interaction effect.

To ensure that layer-specific differences were not influencing our model results, we explored the use of random effects. We used a linear mixed model (glmmTMB function, glmmTMB package (Brooks et al., 2017)) that was identical to the linear model above, with the addition of layer ID as a random slope term. The random slope had a negligible effect on the coefficients and significance of the model terms, indicating that random differences between layers were not influential. Because of this, we decided to continue with the simple linear model for our analysis instead.

2.4.3. Model assessment

For all regression models in our analysis, model fit and assumptions were checked by visually inspecting residual plots, QQ plots, and influential outliers. For the linear mixed model analysis, this was done using the DHARMa package in R (Hartig, 2022). Values of R^2 were calculated manually for all linear models using the adjusted R^2 definition.

3. Results

3.1. BHG – shear frame comparison

Snow layers in our comparison had a wide range of snow properties, including both high and low shear strength and blade hardness values (Table 2). $(\tau_f)_{avg}$ of a snow layer had higher correlation with B_{avg} ($r_s = 0.915, p < 10^{-5}$) than ρ_{avg} ($r_s = 0.820, p < 10^{-5}$), although the difference is small and both variables correlate well. These results are consistent with past studies that show that blade hardness is a better index of snow strength than density (Borstad and McClung, 2011), which has been traditionally used. A linear regression (Fig. 7 B) between B_{avg} and $(\tau_f)_{avg}$ of the 18 snow layers in our comparison fits our data well ($R^2 = 0.94, p < 10^{-11}$). The intercept term was determined to not be significant, so it was set to zero. This relationship can be represented by the equation:

$$(\tau_f)_{avg} = 0.417 B_{avg} \quad (1)$$

where $(\tau_f)_{avg}$ is in kilopascals and B_{avg} is in Newtons. However, our comparison showed that the median CV of the BHG ($CV = 0.207$) was significantly higher ($p < 10^{-5}$) than the median CV of the shear frame ($CV = 0.152$) (Fig. 7 A). This means that more BHG measurements are needed than shear frame measurements to estimate the true mean layer strength with the same precision. This result is unsurprising, since the

Table 2
Properties of the snow layers in our shear frame – BHG comparison, organized by primary crystal form (F). PP, DF, RG, FC, and DH denote precipitation particles, decomposing fragmented, rounded, faceted, and depth hoar crystals, respectively (Fierz et al., 2009). N_{layers} is the number of layers sampled of each crystal form. ρ_{avg}, B_{avg}, and $(\tau_f)_{avg}$ are the average of six 250 cc density measurements, 10 blade hardness measurements, and 10 shear frame measurements, respectively. CV_B and CV_S are the coefficient of variations using the blade hardness gauge and shear frame, respectively. This indicates variation in point measurements relative to their mean for each layer tested.

F	N_{layers}	$\rho_{avg}\left(kg/m^3\right)$	B_{avg} (N)	CV_B	$(\tau_f)_{avg}$ (kPa)	CV_S
PP	1	72	1.3	0.34	0.23	0.22
DF	3	96–241	0.22–3	0.23–0.42	0.098–1.7	0.11–0.26
RG	6	164–336	3.3–11	0.14–0.28	1.1–4.8	0.072–0.19
FC	7	186–314	1.4–6.5	0.12–0.8	0.56–2.4	0.051–0.27
DH	1	280	3.6	0.15	1.2	0.14

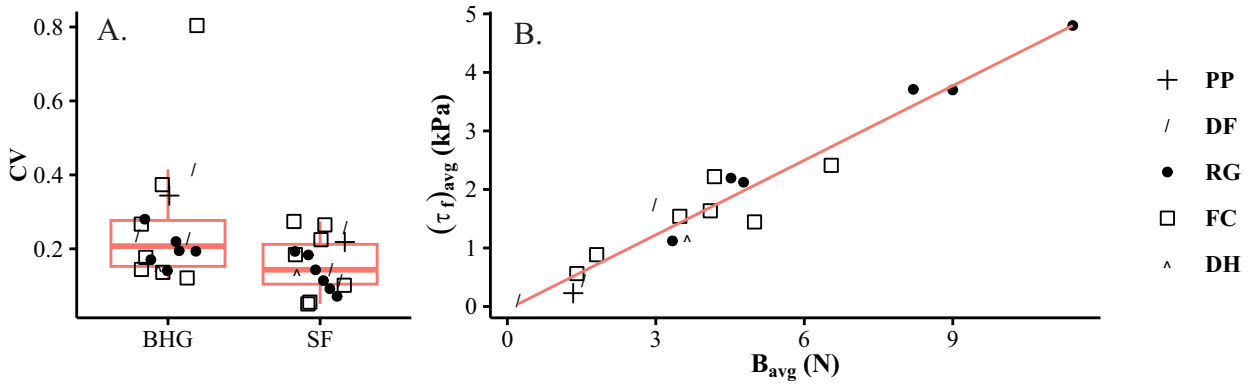

Fig. 7. (A) The coefficient of variation (CV) using the blade hardness gauge (BHG) and shear frame (SF) is shown for all 18 layers in our comparison. We compared the median CV from each instrument because one layer had very high CV using the BHG. (B) The linear regression between B_{avg} (N) and $(\tau_f)_{avg}$ (kPa) is shown ($R^2 = 0.94$). Points in both panels are organized by crystal form (see explanation of codes in Table 2).

100 mm blade samples less layer heterogeneity than the larger shear frame.

3.2. Wet snow strength

Of the 19 snow layers in our analysis, eight were composed of rounded crystals (RG), eight were composed of faceted crystals (FC) which were rounding, and three were composed of decomposing and fragmented crystals (DF). Other primary crystals forms, such as depth hoar, were either not present or did not form the upper layer of a hydraulic barrier during our wetting experiments. This resulted in 135 paired measurements of θ and B in RG layers, 172 in FC layers, and 42 in DF layers (Table 3). θ in these snow layers ranged between 0 and 15 % (Fig. 6) and depended on the effectiveness of the hydraulic barrier at accumulating and laterally distributing water. We were able to take many paired measurements ($N = 146$) at or above $\theta = 7\%$, addressing this data gap from previous studies.

A linear regression using $ln(B)$ as the response and θ, B_{dry}, and F as predictors was significant ($p < 10^{-16}$) and had good fit ($R^2 = 0.853$). E was not significant ($p = 0.31$) and therefore excluded from the final regression. The regression equation of our model can be written as:

$$B = B_{dry}e^{M\theta} \tag{2}$$

where,

$$M = c_1 + c_2 B_{dry} \tag{3}$$

and coefficients c_1 and c_2 depend on the primary crystal form. These coefficients are significant and create a good fit for all three crystal forms in our study (Table 4, Fig. 8). M is a straight line that determines the sign and influences the magnitude of the rate that B changes with respect to θ. When M is negative, B decreases with θ and vice-versa. For all crystal forms, M is inversely proportional to B_{dry}. Although there are significant differences between all crystal forms, coefficient c_2 is not significantly different between RG and FC ($p = 0.54$).

Table 4
Coefficients c_1 and c_2 in eq. 3 and R^2 as they vary with primary crystal form (F). All coefficients are significant ($p < 10^{-10}$).

F	c_1	c_2	R^2
RG	−0.0338	−0.00435	0.83
FC	−0.0726	−0.00487	0.851
DF	0.183	−0.0482	0.839

Since we demonstrated in section 3.1 that there is good agreement between blade hardness and shear frame measurements (eq. 1), we can also write eq. 2 in terms of shear strength:

$$\tau_f = 0.417 B_{dry}e^{M\theta} \tag{4}$$

However, it is important to note that this is an estimate of shear strength which adds additional error and is only applicable when normal stress is low. In Fig. 9, we use eq. 4 to show how our results for FC and RG layers compare to the study of Yamanoi and Endo (2002). This comparison, as well as details about interpreting our blade hardness measurements in terms of shear strength, are expanded upon in section 4.

3.2.1. Rounded and faceted crystals

Of the eight RG layers used in our study, four were composed of recently rounded snow with relatively low dry density ($\rho_{dry} < 250\ kg/m^3$) and four were composed of higher density snow that had been rounding and settling for longer. Apart from one coarse grained layer ($E = 2\ mm$, $\rho_{dry} = 295\ kg/m^3$), all layers were medium to fine grained ($E \leq 1\ mm$) (Fig. 6). Most RG layers ($N = 6$) had $B_{dry} < 7$ N, but two layers had values that were considerably higher (12 N and 18 N) (Fig. 6). The stronger of these two layers was composed of fine crystals ($E = 0.3\ mm$) that were tightly compacted by wind. Qualitative observations indicated that these fine-grained and high-density layers formed the most effective capillary barriers, agreeing with past studies (Avanzi

Table 3
A summary of the snow layers used in our wetting experiments organized by primary crystal form (F). $N_{<7}$ and $N_{>7}$ represent the number of measurements taken below and above $\theta = 7\%$ respectively. N_{tot} is the total number of paired measurements taken for each crystal form. ρ_{dry} is the average of 10 SLF snow sensor measurements taken directly on the plot surface prior to wetting.

F	N_{layers}	N_{tot}	E (mm)	$\rho_{dry}\left(kg/m^3\right)$	B_{dry} (N)	θ (%)	$N_{<7}$	$N_{>7}$
RG	8	135	0.1–2	199–337	2.6–18	0–15	70	65
FC	8	172	0.5–2	220–313	3.4–14	0–13	97	75
DF	3	42	0.3–1	142–176	0.56–1.9	0–9.2	36	6

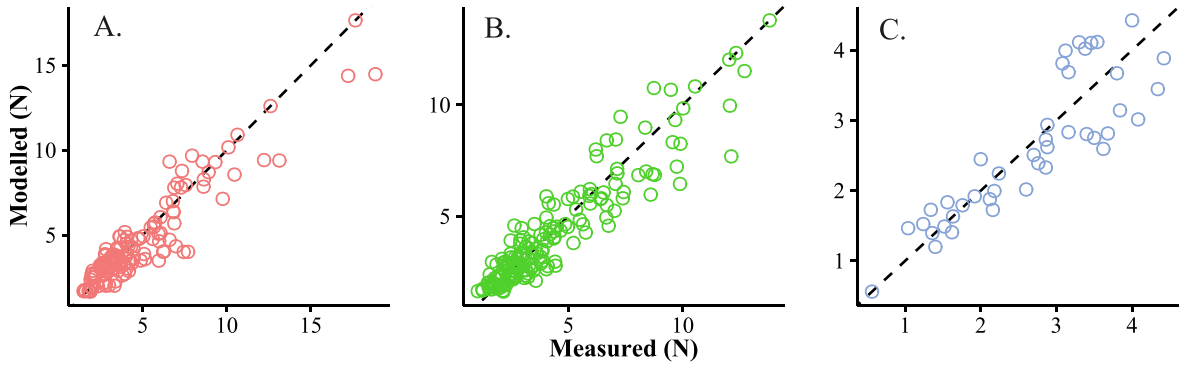

Fig. 8. Modelled wet blade hardness using the regression from our study (eq. 2) against measured values. Graphs A, B, and C show data for RG ($R^2 = 0.830$, $N_{tot} = 135$), FC ($R^2 = 0.851$, $N_{tot} = 172$), and DF ($R^2 = 0.839$, $N_{tot} = 42$) crystal forms, respectively. The dashed line is 1–1. Note the differences in axes limits to better visualize the point distribution in each panel.

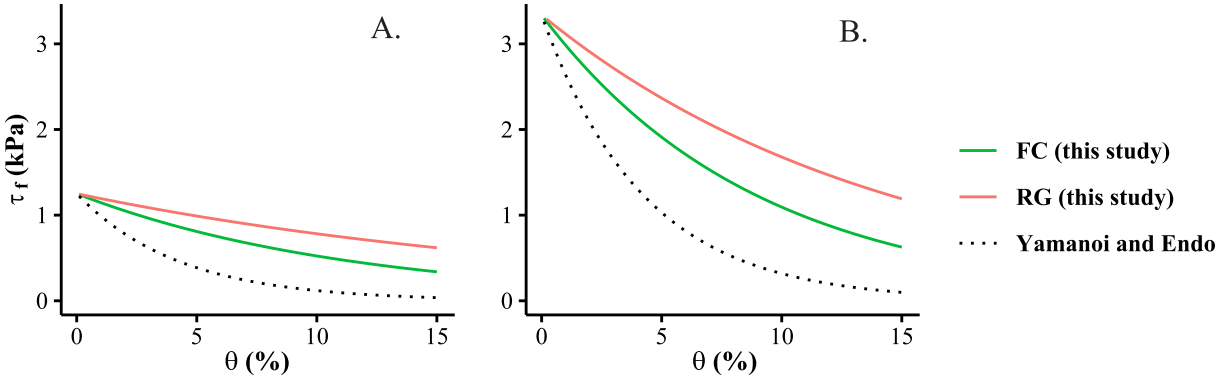

Fig. 9. Using eq. 4 to compare our regression for FC and RG layers to the regression from Yamanoi and Endo (2002). (A) $B_{dry} = 3$ N (or $\tau_f = 1.3$ *kPa*, eq. 1) and (B) $B_{dry} = 8$ N (or $\tau_f = 3.3$ *kPa*, eq. 1). For a given dry strength, the Yamanoi and Endo regression does not vary with crystal form and decreases at a larger rate with respect to θ.

et al., 2016; Waldner et al., 2004; Webb et al., 2018). This was also the case for our FC layers, although they seemed to produce less effective capillary barriers than the RG layers overall.

Due to the continental snow climate of our study area, FC crystals often dominated the snowpack at our plots. However, due to the mild temperatures during our experiments, these layers were at various stages of rounding. FC layers used in our study had dry densities ranging between 220 and 313 kg/m^3 and crystal sizes ranging between 0.5 and 2 mm (Fig. 6). Three of the FC layers had undergone very significant rounding, resulting in relatively high dry blade hardness ($B_{dry} > 10$ N). Despite this, the chain-like structure of crystals formed by kinetic metamorphism (Pinzer et al., 2012) was still present in these layers. The remaining five layers had B_{dry} between 3.4 and 7.1 N.

Our analysis revealed that both RG and FC layers in our study continuously decreased in strength as θ increased (Table 4, $p < 10^{-10}$), even when θ was low (< 6%). Our negative exponential regression (Fig. 9) demonstrates that weakening rates are large at low θ and then become smaller as θ increases. Fig. 10 illustrates both the change in blade hardness due to θ ($B - B_{dry}$, Fig. 10 A) and the proportional significance of this change (B/B_{dry}, Fig. 10 B), for all crystal forms and values of B_{dry} measured in our study. The dashed lines in both graphs represent no change. When $\theta = 6.5\%$ (mean θ measured for RG and FC layers), B is predicted to be 0.4–0.75 times its dry value (Fig. 10 B). The amount that B decreased with respect to θ increased with B_{dry} and depended on crystal form (Fig. 10 A). At a given B_{dry} and θ, RG layers decreased less in B than FC layers. These differences are shown in Fig. 10 A by almost parallel but vertically offset lines. Unlike FC layers, some RG layers had B measurements above B_{dry} at low θ (< 6%). These measurements were generally limited (points above 0 in plot A or above 1 in plot B, Fig. 10) but one layer was a notable exception (6 measurements). This was the weakest RG layer measured when dry ($B_{dry} = 2.6$ N) and had a secondary form listed as DF. Although these limited measurements showing strengthening are possibly meaningful, they are poorly represented by our regression.

3.2.2. *Decomposing fragmented crystals*

DF crystals were the least common crystal form in our dataset with only 3 layers included ($N = 42$ samples). Although subtle textural differences in this snow type commonly create capillary barriers (Peitzsch et al., 2008), we found that they were difficult to identify and target with our wetting method. Furthermore, these layers were close to the snow surface and often very cold from radiative loss the previous night. This made it difficult to sufficiently warm these layers while also shading them from incoming solar radiation. The three DF layers that we managed to measure had dry densities ranging between 142 and 176 kg/m^3 and crystal sizes ranging between 0.3 and 1 mm (Fig. 5). B_{dry} varied little, between 0.56 and 1.9 N.

Unlike RG and FC layers, DF layers in our study continuously increased in strength as θ increased (Table 4, $p < 10^{-10}$). When $\theta = 5.7\%$ (mean θ measured for DF layers), B is predicted to be 1.7–2.5 times its dry value (Fig. 10 B) – a substantial difference compared with RG and FC layers. Despite B_{dry} varying very little, it still had a significant effect in our regression. The amount that B increased with respect to θ increased with B_{dry} (positively sloped line in Fig. 10 A). However, the proportional significance of these increases in B decreased with B_{dry} (negatively sloped line in Fig. 10 B). Since the number of DF layers in our analysis is so small, the validity of these relationships with B_{dry} is unclear.

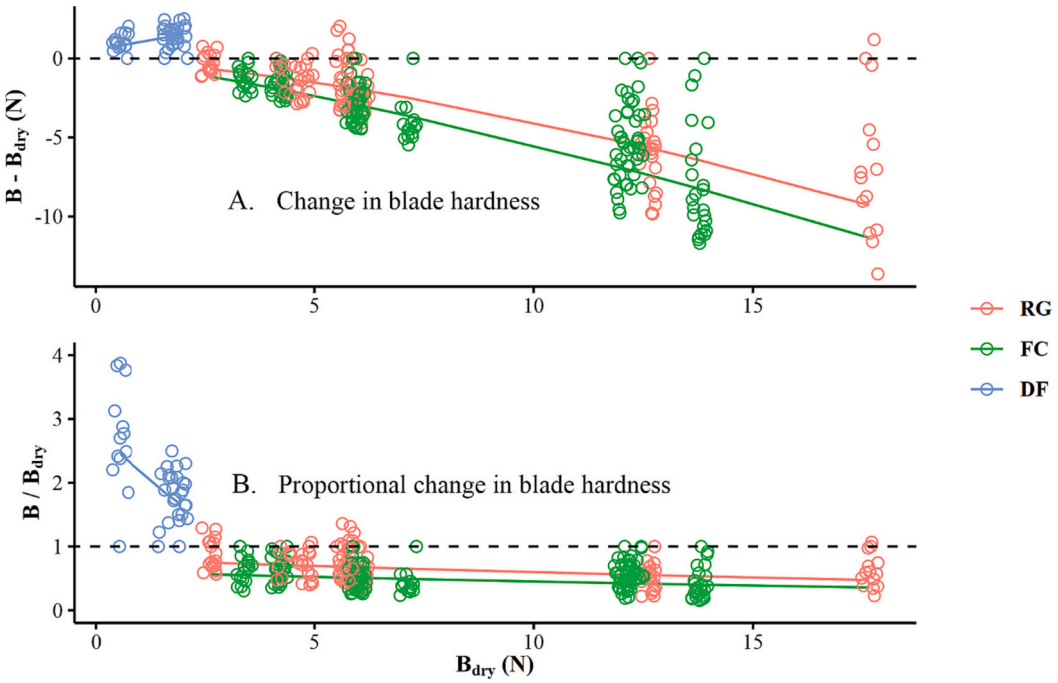

Fig. 10. Raw data that doesn't account for the variance in θ is plotted on top of both graphs. (A) This graph shows how the predicted change in blade hardness ($B - B_{dry}$) varies with B_{dry}, when θ is set to its mean value (6.5% for RG and FC, 5.7% for DF). The negatively sloped lines for RG and FC layers demonstrate that weakening due to θ increases with B_{dry} for these crystal forms. (B) The predicted proportional change in blade hardness (B/B_{dry}) is plotted against B_{dry}, when θ is set to the same mean values. In some DF snow layers, wet measurements were up to 4 times larger than their initial dry value, illustrating how significant some strength changes were in this crystal form.

4. Discussion

4.1. Interpreting BHG measurements in terms of shear strength

Although our comparison between the BHG and shear frame was done in dry snow for convenience, we expect and suggest that the same relationship will hold in wet snow. However, since layer heterogeneity often increases after wetting due to preferential flow (Williams et al., 2010), we expect that more BHG measurements in wet snow would have been necessary to achieve the same result, and that a wider range in uncertainty would have been displayed. In the following discussion, we leverage the high correlation between the two instruments to interpret our BHG measurements in terms of shear strength when compressive stress is low. Under these conditions, the usual Mohr-Coulomb failure criteria is known to work well (Podolskiy et al., 2015; Reiweger et al., 2015; Roch, 1965; Zeidler and Jamieson, 2006):

$$\tau_f = c + \sigma_f tan\Phi \tag{5}$$

where shear stress at failure (τ_f) is a function of normal stress (σ_f), cohesion (c), and the internal angle of friction (Φ). In dry snow, cohesion comes from the size and number of ice bonds connecting crystals (Podolskiy et al., 2015) and Φ determines the frictional resistance between crystals, which varies with snow type (Podolskiy et al., 2015; Roch, 1965). After wetting, both c and Φ become a function of θ due to bond melting (Colbeck, 1973) and rapid changes to crystal shape and density (Brun, 1989; Coléou and Lesaffre, 1998; Marshall et al., 1999). Additionally, there is an increase in normal stress due to capillary pressure that also varies with θ. In sand, which acts in similar ways to snow when wet (Yamaguchi et al., 2010), this can be accounted for by replacing σ_f in eq. 5 with an effective normal stress term σ_f' (Lu and Likos, 2004):

$$\sigma_f' = \sigma_f + X_\theta h_\theta \tag{6}$$

where h_θ is capillary suction (difference between pore air and water pressures) and X_θ is a function between 0 (dry) and 1 (fully saturated) that adjusts the area over which capillary suction acts (Bishop, 1959). However, since we removed all but ~1 cm of overlying snow before measurement, we can assume $\sigma_f \cong 0$. Thus, for our measurements in wet snow at a given θ, we can rewrite eq. 5 as:

$$\tau_f = c_\theta + X_\theta h_\theta tan\Phi_\theta \tag{7}$$

where c_θ is cohesion from any un-melted bonds and Φ_θ is the new internal angle of friction after short-term (< 2 h) wet snow metamorphism has occurred. $X_\theta h_\theta tan\Phi_\theta$ represents the addition of shear strength from capillary cohesion and will be used in the following sections.

4.2. Properties controlling strength changes in wet snow

4.2.1. Rounded and faceted crystals

Both the RG and rounding FC layers in our study generally decreased in strength as soon as they became wet, and the amount of weakening for a given θ increased with B_{dry}. Although eq. 4 shows a similar trend as the study of Yamanoi and Endo (2002), there are some critical differences (Fig. 9). For a given dry strength, the Yamanoi and Endo regression does not vary with crystal form, contrary to our results. Their regression also predicts weakening rates that are considerably larger than ours. However, detailed comparisons are difficult to make since their study sampled naturally wetted snow that had likely been wet for longer, allowing more time for metamorphism and weakening to occur. Their study also used a permittivity device with a larger volume of influence, an unconventional style of shear frame, and they did not adjust for frame size effects.

Previous theoretical work describing the bond melting process idealizes wet snow as having evenly sized pore spaces that are equally saturated (Colbeck, 1973). Under this model, there is no bond melting until a particular θ is reached, and then it occurs all at once. However, in natural snow each pore space has a unique geometry and smaller pores

will saturate more than larger ones when wetted. Therefore, even when θ is low overall, some pores may be sufficiently saturated to melt neighboring bonds. This interpretation of wet snow agrees better with our results and those from previous studies (Techel et al., 2011; Yamanoi and Endo, 2002) that show a continuous weakening beginning at low θ. It also facilitates a better understanding of the effect that B_{dry} has on weakening rates. Snow with higher dry strength has greater bond density and, therefore, more bonds neighboring pore spaces where melting can occur. Conversely, snow with low dry strength experiences smaller weakening rates since bonds neighboring saturated pores are fewer at a given θ.

The actual magnitude of weakening from bond melting is difficult to quantify since the effect of capillary cohesion is simultaneously present. To help clarify this, we use the definition in eq. 7 to approximate capillary cohesion in our highest density RG layer ($\rho_{dry} = 337\ kg/m^3$). h_θ was calculated using the Van Genuchten (Van Genuchten, 1980) parameterization, setting $\alpha = 20$ and $n = 4$. These values are approximately equal to those measured in a natural RG layer with similar density ($\rho_{dry} = 309\ kg/m^3$) (Yamaguchi et al., 2012). We use $X_\theta = (\theta - \theta_r)/(\theta_s - \theta_r)$ (Lu and Likos, 2004), where θ_r is the residual θ (θ as $h \to \infty$) and θ_s is the θ at saturation. We assume $\theta_r = 0.02$ and θ_s is 10% less than porosity (Yamaguchi et al., 2010). We also assume a constant Φ_θ of 37° (Chandel et al., 2014), since it is unclear how it will change with respect to θ. Comparing this estimate of capillary cohesion to the predicted shear strength using eq. 4, some interesting trends emerge (Fig. 11). As capillary cohesion increases, weakening rates decrease in a similar manner. This suggests that capillary cohesion may play an important role in moderating strength loss from bond melting. Furthermore, capillary cohesion and shear strength converge near $\theta = 15\%$, implying that all bonds have been melted ($c_\theta \cong 0$, eq. 7). Since $\theta = 15\%$ is well into the funicular regime, this transition point makes sense. However, interpretations using this estimate of capillary cohesion are limited. Assuming constant Φ_θ is inaccurate and h_θ is likely overestimated since a drying path was used for measurement (Yamaguchi et al., 2010). Since wet snow experiences hysteresis, h_θ is lower when wetted, as seen in our study, than dried for a given θ (Leroux and Pomeroy, 2017).

Although RG and FC layers behaved similarly, our analysis shows that FC layers decreased in strength significantly more than RG layers at the same θ. This is consistent with other observations (Marienthal et al., 2012; Reardon, 2008; Techel et al., 2011) that the strength of faceted snow is particularly sensitive to liquid water. Theory has shown that small temperature gradients between wet crystal surfaces that drive bond melting may increase quadratically with the ratio of crystal to bond radius (Colbeck, 1973). Since this ratio can be particularly high in faceted snow (Brown et al., 2001), bond melting may occur earlier and more quickly than in other snow types. For a given θ and B_{dry}, capillary cohesion will also be different in faceted than rounded snow, since kinetic metamorphism creates a unique pore structure (Pinzer et al., 2012). However, until h_θ is parameterized in faceted snow, the extent to which this difference can explain our results is unclear.

4.2.2. *Decomposing and fragmented crystals*

To the authors' knowledge, our measurements in DF layers are the first time that significant increases in wet snow strength have been demonstrated. This result is related to the fact that snow that has recently fallen becomes particularly sticky when wet – something that is perhaps intuitive for many people in snowy climates. This "stickiness" is a sign of high h_θ, suggesting that capillary cohesion is also high in this snow type. Additionally, DF snow is weak when dry, so there are fewer bonds to melt when wetted. Thus, weakening from bond melting is likely exceeded by strengthening from capillary cohesion, resulting in the trend that we observed. This may also explain why one RG layer in our study, which had low B_{dry} and a secondary form of DF, also showed signs of increasing strength at low θ. However, given the limited number of DF layers sampled ($N = 3$ layers / $N = 42$ samples), further testing is required to verify these interpretations. We also note that recently wetted DF snow is not a commonly cited weak layer for wet slab avalanches (Jamieson et al., 2001; Marienthal et al., 2012), so this short term (< 2 h) gain in strength may have limited significance.

4.3. *Limitations*

It is important to note that there is a temporal component of wet snow strength that is not addressed in this study. We measure snow layers that have recently become wet (< 2 h) and do not account for longer-term metamorphic changes affecting snow strength. This caveat is particularly important for DF snow, since it rapidly densifies and rounds when wet (Marshall et al., 1999) and will likely behave similarly to RG snow at longer time scales. Another consideration is whether the high θ seen in our study could be achieved in such a short time frame during a natural wetting cycle. The rate at which we supplied liquid water to the snow surface (~30 mm/h) is larger than typical melt or rain events. However, the high rate at which liquid water arrived at the hydraulic barrier agrees with observations of preferential flow in more natural settings (e.g. Waldner et al., 2004).

There are also inherent limitations to our measurement methods. Although θ measurements were targeted at portions of evenly wetted snow, they were still influenced by less wet or dry snow above and below the hydraulic barrier. This means that θ is likely an underestimate of the true θ where BHG measurements were taken. However, this discrepancy should be minimal in comparison to other studies since our instruments have a smaller volume of influence. Other issues arise from calculating θ using permittivity, which relies on empirical relationships that are known to cause errors of up to $\theta = 2\%$ (Webb et al., 2021). However, methods that don't rely on permittivity, like calorimetry, are destructive

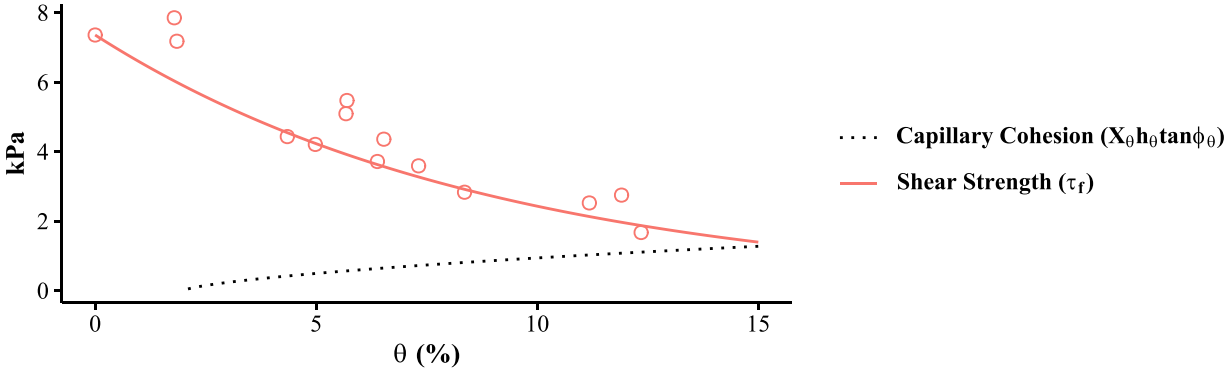

Fig. 11. Estimate of capillary cohesion ($X_\theta h_\theta tan\Phi_\theta$, eq. 7) and shear strength (τ_f, eq. 4) for the highest density ($\rho_{dry} = 337\ kg/m^3$) RG layer in our study. This layer had $B_{dry} = 17.7$ N (or $\tau_f = 7.36\ kPa$, eq. 1). Raw measurements that are converted to shear strength using eq. 1 are also shown. Of particular interest is the convergence point of these two lines, near $\theta = 15\%$. According to eq. 7, this should occur when all bonds have melted ($c_\theta \cong 0$).

and don't allow for paired strength measurements of the same sample volume.

Using manual observations of crystal form as a predictor of wet snow strength could also be problematic. We expect that the characteristics of individual crystals are less important than the geometry of pore spaces, which may be better represented by measures such as specific surface area (Hirashima et al., 2017). Despite these limitations, our results show that well-fitting regressions of wet snow strength are still possible using relatively simple methods and snow properties that are easily measured by avalanche professionals in the field.

5. Conclusion

A blade hardness gauge (BHG) and SLF snow sensor were used to take 349 targeted paired measurements of strength and θ, respectively, in the snow above 19 manually wetted hydraulic (capillary) barriers. In these layers, many θ measurements were taken above 7%, addressing this important data gap in the literature. Using a multiple regression analysis, we developed an expression for the blade hardness of manually wetted snow as a function of θ, crystal form, and blade hardness prior to wetting. Additionally, we showed that BHG and shear frame measurements are highly correlated (216 measurements from each instrument taken across 18 different dry snow layers), allowing us to interpret our regression in terms of shear strength when compressive stress is low.

Snow composed of rounds or rounding faceted crystals generally decreased in strength with increasing θ. Counterintuitively, the magnitude of weakening at a given θ increased with dry strength in these snow types. This suggests that snow layers that are strong when dry could still become failure layers when wetted, especially if they sit above effective hydraulic barriers. Furthermore, weakening was greater in rounding faceted than rounded snow, for a given θ and dry strength. This agrees with both anecdotal and experimental evidence that associate faceted snow layers with wet slab avalanche activity. Decomposing and fragmented snow behaved differently and increased in strength with increasing θ. However, over longer periods, this result may no longer hold since wet decomposing and fragmented snow will metamorphose to rounds. Further investigation is necessary to constrain this temporal component.

Currently, our results can only be used to estimate the shear strength provided by un-melted bonds and capillary suction, shortly after wetting. Quantifying how other mechanical parameters change when wet, like frictional resistance (i.e., Φ_θ) and compressive strength, is necessary to model the failure of weak snow layers during wet slab avalanche release. However, our results still demonstrate that short-term (< 2 h) changes in snow strength due to increasing liquid water content are significantly different between snow types. These differences can be empirically modelled using easily measured dry snow properties, which could allow avalanche forecasters to be more selective when identifying failure layers in advance of a wetting event.

Funding

This work was supported in part by the University of New Mexico Graduate and Professional Student Association.

CRediT authorship contribution statement

Mikael Schlumpf: Conceptualization, Methodology, Validation, Formal analysis, Investigation, Writing – original draft, Writing – review & editing. **Jordy Hendrikx:** Conceptualization, Methodology, Resources, Writing – review & editing. **John Stormont:** Conceptualization, Writing – review & editing. **Ryan Webb:** Conceptualization, Methodology, Validation, Resources, Writing – review & editing, Supervision.

Declaration of Competing Interest

The authors declare that they have no known competing financial interests or personal relationships that could have appeared to influence the work reported in this paper.

Data availability

Datasets related to this research can be found at https://doi.org/10.5281/zenodo.8436295, an open-source online data repository hosted by Zenodo

Acknowledgements

We would like to thank the editor, Nicolas Eckert, and the two reviewers who provided constructive comments that helped improve this manuscript. We would also like to thank Mark Stone and Adrian Marziliano for providing valuable discussions and feedback. We are grateful to the University of New Mexico Graduate and Professional Student Association for partly funding this research.

References

Avanzi, F., Hirashima, H., Yamaguchi, S., Katsushima, T., De Michele, C., 2016. Observations of capillary barriers and preferential flow in layered snow during cold laboratory experiments. Cryosphere 10, 2013–2026. https://doi.org/10.5194/tc-10-2013-2016.

Baggi, S., Schweizer, J., 2009. Characteristics of wet-snow avalanche activity: 20 years of observations from a high alpine valley (Dischma, Switzerland). Nat. Hazards 50, 97–108. https://doi.org/10.1007/s11069-008-9322-7.

Barsevskis, P., Paetkau, M., 2022. Snow Characteristics with the Blade Hardness Gauge.

Bhutiyani, M., 1996. Field investigations on meltwater percolation and its effect on shear strength of wet snow. Proc. Int. Symposium Snow 94, 200–206.

Birkeland, K.W., 1998. Terminology and predominant processes associated with the formation of weak layers of near-surface faceted crystals in the mountain snowpack. Arct. Alp. Res. 30, 193–199. https://doi.org/10.1080/00040851.1998.12002891.

Birkeland, K.W., Kronholm, K., Logan, S., Schweizer, J., 2006. Field measurements of sintering after fracture of snowpack weak layers. Geophys. Res. Lett. 33 https://doi.org/10.1029/2005GL025104.

Bishop, 1959. The principle of effective stress. Teknisk Ukeblad 39, 859–863.

Borstad, C.P., McClung, D.M., 2011. Thin-blade penetration resistance and snow strength. J. Glaciol. 57, 325–336. https://doi.org/10.3189/002214311796405924.

Borstad, C.P., McClung, D.M., 2013. A higher-order method for determining quasi-brittle tensile fracture parameters governing the release of slab avalanches and a new tool for in situ indexing. Case Rep. Med. 118, 900–912. https://doi.org/10.1002/jgrf.20065.

Brooks, M.E., Kristensen, K., van Benthem, K.J., Magnusson, A., Berg, C.W., Nielsen, A., Skaug, H.J., Mächler, M., Bolker, B.M., 2017. glmmTMB balances speed and flexibility among packages for zero-inflated generalized linear mixed modeling. R Journal 9, 378–400.

Brown, R.L., Satyawali, P.K., Lehning, M., Bartelt, P., 2001. Modeling the changes in microstructure of snow during metamorphism. Cold Regions Science and Technology, ISSW 2000:International Snow Science Workshop 33, pp. 91–101. https://doi.org/10.1016/S0165-232X(01)00032-5.

Brun, E., 1989. Investigation on wet-snow metamorphism in respect of liquid-water content. Ann. Glaciol. 13, 22–26. https://doi.org/10.3189/S0260305500007576.

Brun, E., Rey, L., 1987. Field study on snow mechanical properties with special regard to liquid water content. Symposium at Davos 1986—Avalanche Formation, Movement and Effects, IAHS Publ., 162. International Association of Hydrological Sciences, Wallingford, Oxfordshire, UK, pp. 183–193.

Castebrunet, H., Eckert, N., Giraud, G., Durand, Y., Morin, S., 2014. Projected changes of snow conditions and avalanche activity in a warming climate: the French Alps over the 2020-2050 and 2070-2100 periods. Cryosphere 8, 1673–1697. https://doi.org/10.5194/tc-8-1673-2014.

Chandel, C., Mahajan, P., Srivastava, P.K., Kumar, V., 2014. The behaviour of snow under the effect of combined compressive and shear loading. Curr. Sci. 107, 888–894.

Colbeck, S.C., 1973. Theory of metamorphism of wet snow. Research Report Vol. 311 U. S. Army Corps of Engineers, Cold Regions Research and Engineering Laboratory: Hanover, NH; 13.

Coléou, C., Lesaffre, B., 1998. Irreducible water saturation in snow: experimental results in a cold laboratory. Ann. Glaciol. 26, 64–68. https://doi.org/10.3189/1998AoG26-1-64-68.

Conway, H., Raymond, C.F., 1993. Snow stability during rain. J. Glaciol. 39, 635–642. https://doi.org/10.3189/S0022143000016531.

Denoth, A., 1980. The Pendular-Funicular Liquid transition in Snow. J. Glaciol. 25, 93–98. https://doi.org/10.3189/S0022143000010315.

Eiriksson, D., Whitson, M., Luce, C.H., Marshall, H.P., Bradford, J., Benner, S.G., Black, T., Hetrick, H., McNamara, J.P., 2013. An evaluation of the hydrologic

relevance of lateral flow in snow at hillslope and catchment scales. Hydrol. Process. 27, 640–654. https://doi.org/10.1002/hyp.9666.
Fierz, C., Fohn, P., 1994. Long-term Observations of the Water Content of an Alpine Snowpack. Proceedings of the International Snow Science Workshop, Snowbird, USA, pp. 117–131.
Fierz, Armstrong, Durand, Etchevers, Greene, McClung, Nishimura, Satyawali, Sokratov, 2009. The International Classification for Seasonal Snow on the Ground. UNESCO-IHP, Paris.
Föhn, P., 1987. The stability index and various triggering mechanisms. Symposium at Davos 1986—Avalanche Formation, Movement and Effects. IAHS Publ. 162, 195–214.
Fohn, P., Camponovo, C., 1997. Improvements by Measuring Shear Strength of Weak Layers. Proceedings of the International Snow Science Workshop, Banff, Canada, pp. 158–162.
FPGA Company, 2018. SLF Snow Sensor Manual.
Gaume, J., van Herwijnen, A., Chambon, G., Wever, N., Schweizer, J., 2017. Snow fracture in relation to slab avalanche release: critical state for the onset of crack propagation. Cryosphere 11, 217–228. https://doi.org/10.5194/tc-11-217-2017.
Hartig, F., 2022. DHARMa: Residual Diagnostics for Hierarchical (Multi-Level / Mixed) Regression Models.
Heierli, J., Gumbsch, P., Zaiser, M., 2008. Anticrack nucleation as triggering mechanism for snow slab avalanches. Science 321, 240–243. https://doi.org/10.1126/science.1153948.
Hendrikx, J., Jones, A., Argue, C., Buhler, R., Jamieson, B., Goodrich, J., 2022. The Potential Impacts of Climate Change on Snow Avalanche Hazards on the Trans-Canada Highway in Glacier National Park. XVI PIARC World Winter Service and Road Resilience Congress, Calgary, Canada.
Hirashima, H., Avanzi, F., Yamaguchi, S., 2017. Liquid water infiltration into a layered snowpack: evaluation of a 3-D water transport model with laboratory experiments. Hydrol. Earth Syst. Sci. 21, 5503–5515. https://doi.org/10.5194/hess-21-5503-2017.
Jamieson, Johnston, C.D., 2001. Evaluation of the shear frame test for weak snowpack layers. Ann. Glaciol. 32, 59–69. https://doi.org/10.3189/172756401781819472.
Jamieson, B., Geldsetzer, T., Stethem, C., 2001. Forecasting for deep slab avalanches. Cold Reg. Sci. Technol. 33, 275–290. https://doi.org/10.1016/S0165-232X(01)00056-8.
Johnson, J.B., Schneebeli, M., 1998. Snow strength penetrometer. US5831161A.
Kattelmann, R., 1985. Wet Slab Instability. Proceedings of the International Snow Science Workshop, Aspen, Colorado, USA, pp. 102–108.
Lazar, B., Williams, M., 2008. Climate change in western ski areas: Potential changes in the timing of wet avalanches and snow quality for the Aspen ski area in the years 2030 and 2100. Cold Regions Science and Technology, International Snow Science Workshop (ISSW) 2006 51, pp. 219–228. https://doi.org/10.1016/j.coldregions.2007.03.015.
Leroux, N.R., Pomeroy, J.W., 2017. Modelling capillary hysteresis effects on preferential flow through melting and cold layered snowpacks. Adv. Water Resour. 107, 250–264. https://doi.org/10.1016/j.advwatres.2017.06.024.
Lu, N., Likos, W.J., 2004. Shear Strength. In: Unsaturated Soil Mechanics. John Wiley & Sons, Inc., pp. 220–265
Marienthal, A., Hendrikx, J., Chabot, D., Maleski, P., Birkeland, K., 2012. Depth Hoar, Avalanches, and Wet Slabs: A case study of the historic March 2012 wet slab avalanche cycle at Bridger Bowl, Montana. Proceedings of the International Snow Science Workshop, Anchorage, USA.
Marshall, H.P., Conway, H., Rasmussen, L.A., 1999. Snow densification during rain. Cold Reg. Sci. Technol. 30, 35–41. https://doi.org/10.1016/S0165-232X(99)00011-7.
Mitterer, C., Schweizer, J., 2013. Analysis of the snow-atmosphere energy balance during wet-snow instabilities and implications for avalanche prediction. Cryosphere 7, 205–216. https://doi.org/10.5194/tc-7-205-2013.
Mitterer, C., Schweizer, J., 2014. Comparing models of different levels of complexity for the prediction of wet-snow avalanches. Proceedings of the International Snow Science Workshop, Banff, Canada, pp. 9–14.
Peitzsch, Birkeland, K., Hansen, K., 2008. Water movement and capillary barriers in a stratified and inclined snowpack. Proceedings of the International Snow Science Workshop, Whistler, Canada, pp. 179–187.
Peitzsch, E.H., Hendrikx, J., Fagre, D.B., Reardon, B., 2012. Examining spring wet slab and glide avalanche occurrence along the Going-to-the-Sun Road corridor, Glacier National Park, Montana, USA. Cold Reg. Sci. Technol. 78, 73–81. https://doi.org/10.1016/j.coldregions.2012.01.012.
Perla, R., Beck, T.M.H., Cheng, T.T., 1982. The shear strength index of alpine snow. Cold Reg. Sci. Technol. 6, 11–20. https://doi.org/10.1016/0165-232X(82)90040-4.
Pielmeier, C., Techel, F., Marty, C., Stucki, T., 2013. Wet snow avalanche activity in the Swiss Alps – trend analysis for mid-winter season. Proceedings of the International Snow Science Workshop, Grenoble and Chamonix, France, pp. 1240–1246.
Pinzer, B.R., Schneebeli, M., Kaempfer, T.U., 2012. Vapor flux and recrystallization during dry snow metamorphism under a steady temperature gradient as observed by time-lapse micro-tomography. Cryosphere 6, 1141–1155. https://doi.org/10.5194/tc-6-1141-2012.
Podolskiy, E.A., Chambon, G., Naaim, M., Gaume, J., 2015. Evaluating snow weak-layer failure parameters through inverse finite element modelling of shaking-platform experiments. Nat. Hazards Earth Syst. Sci. 15, 119–134. https://doi.org/10.5194/nhess-15-119-2015.
Raymond, C.F., Tusima, K., 1979. Grain Coarsening of Water-Saturated Snow. J. Glaciol. 22, 83–105. https://doi.org/10.3189/S0022143000014076.
Reardon, B., 2008. A conceptual model of wet slab avalanche forecasting. Avalanche Rev. 26, 18–19.
Reiweger, I., Gaume, J., Schweizer, J., 2015. A new mixed-mode failure criterion for weak snowpack layers. Geophys. Res. Lett. 42, 1427–1432. https://doi.org/10.1002/2014GL062780.
Roch, A., 1965. Les Variations de la Resistance de la Neige. Int. Assoc. Sci. Hydrol. Publ. 69, 86–99.
Schlumpf, M., Hendrikx, J., Stormont, J., Webb, R., 2023. Regression Datasets: Strength as a Function of Liquid Water Content in Different Snow Types. https://doi.org/10.5281/zenodo.8436295.
Schneebeli, M., 1995. Development and stability of preferential flow paths in a layered snowpack. IAHS-AIHS Publ. 228, 89–96.
Schweizer, J., 1998. Laboratory experiments on shear failure of snow. Ann. Glaciol. 26, 97–102. https://doi.org/10.3189/1998AoG26-1-97-102.
Schweizer, J., Bruce Jamieson, J., Schneebeli, M., 2003. Snow avalanche formation. Rev. Geophys. 41 https://doi.org/10.1029/2002RG000123.
Sinickas, A., Jamieson, B., Maes, M.A., 2016. Snow avalanches in western Canada: investigating change in occurrence rates and implications for risk assessment and mitigation. Struct. Infrastruct. Eng. 12, 490–498. https://doi.org/10.1080/15732479.2015.1020495.
Sommerfeld, R.A., 1980. Statistical models of snow strength. J. Glaciol. 26, 217–223. https://doi.org/10.3189/S0022143000010753.
Sommerfeld, R.A., 1984. Instructions for using the 250 cm2 shear frame to evaluate the strength of a buried snow surface. USDA Forest Service research note RM-446, pp. 1–6.
Techel, F., Pielmeier, C., 2011. Point observations of liquid water content in wet snow – investigating methodical, spatial and temporal aspects. Cryosphere 5, 405–418. https://doi.org/10.5194/tc-5-405-2011.
Techel, F., Pielmeier, C., Schneebeli, M., 2011. Microstructural resistance of snow following first wetting. Cold Reg. Sci. Technol. 65, 382–391. https://doi.org/10.1016/j.coldregions.2010.12.006.
Van Genuchten, 1980. A Closed-form Equation for Predicting the Hydraulic Conductivity of Unsaturated Soils. Soil Science Society of America Journal 44, 892–898. https://doi.org/10.2136/sssaj1980.03615995004400050002x.
van Herwijnen, A., Schweizer, J., Heierli, J., 2010. Measurement of the deformation field associated with fracture propagation in weak snowpack layers. J. Geophys. Res. Earth 115. https://doi.org/10.1029/2009JF001515.
Waldner, P.A., Schneebeli, M., Schultze-Zimmermann, U., Flühler, H., 2004. Effect of snow structure on water flow and solute transport. Hydrol. Process. 18, 1271–1290. https://doi.org/10.1002/hyp.1401.
Webb, R.W., Fassnacht, S.R., Gooseff, M.N., Webb, S.W., 2018. The presence of hydraulic barriers in layered snowpacks: TOUGH2 simulations and estimated diversion lengths. Transp. Porous Media 123, 457–476. https://doi.org/10.1007/s11242-018-1079-1.
Webb, Marziliano, A., McGrath, D., Bonnell, R., Meehan, T.G., Vuyovich, C., Marshall, H.-P., 2021. In situ determination of dry and wet snow permittivity: improving equations for low frequency radar applications. Remote Sens. 13, 4617. https://doi.org/10.3390/rs13224617.
Wever, N., Vera Valero, C., Fierz, C., 2016. Assessing wet snow avalanche activity using detailed physics based snowpack simulations. Geophys. Res. Lett. 43, 5732–5740. https://doi.org/10.1002/2016GL068428.
Wever, N., Vera Valero, C., Techel, F., 2018. Coupled snow cover and avalanche dynamics simulations to evaluate wet snow avalanche activity. J. Geophys. Res. Earth 123, 1772–1796. https://doi.org/10.1029/2017JF004515.
Williams, M.W., Erickson, T.A., Petrzelka, J.L., 2010. Visualizing meltwater flow through snow at the centimetre-to-metre scale using a snow guillotine. Hydrol. Process. 24, 2098–2110. https://doi.org/10.1002/hyp.7630.
Yamaguchi, S., Katsushima, T., Sato, A., Kumakura, T., 2010. Water retention curve of snow with different grain sizes. Cold Regions Science and Technology, International Snow Science Workshop 2009 Davos 64, pp. 87–93. https://doi.org/10.1016/j.coldregions.2010.05.008.
Yamaguchi, S., Watanabe, K., Katsushima, T., Sato, A., Kumakura, T., 2012. Dependence of the water retention curve of snow on snow characteristics. Ann. Glaciol. 53, 6–12. https://doi.org/10.3189/2012AoG61A001.
Yamanoi, K., Endo, Y., 2002. Dependence of shear strength of snow cover on density and water content. J. Japan. Soc. Snow Ice 64, 443–451. https://doi.org/10.5331/seppyo.64.443.
Zeidler, A., Jamieson, B., 2006. Refinements of empirical models to forecast the shear strength of persistent weak snow layers PART a: layers of faceted crystals. Cold Reg. Sci. Technol. 44, 194–205. https://doi.org/10.1016/j.coldregions.2005.11.005.